ADVANCED ENERGY MATERIALS
www.advenergymat.de

Rear Surface Passivation for Ink-Based, Submicron $CuIn(S, Se)_2$ Solar Cells

*Sunil Suresh, Abraha T. Gidey, Towhid H. Chowdhury, Sachin R. Rondiya, Li Tao, Jian Liu, Bart Vermang, and Alexander R. Uhl**

A *N*, *N*-dimethylformamide and thiourea-based route is developed to fabricate submicron (0.55 and 0.75 µm) thick $CuIn(S,Se)_2$ (CISSe) thin films for photovoltaic applications, addressing challenges of material usage, throughput, and manufacturing costs. However, reducing the absorber film thickness below 1 µm in a regular CISSe solar cell decreases the device efficiency due to losses at the highly-recombinative, and mediocre-reflective Mo/CISSe rear interface. For the first time, to mitigate the rear recombination losses, a novel rear contacting structure involving a surface passivation layer and point contact openings is developed for solution processed CISSe films and demonstrated in tangible devices. An atomic layer deposited Al_2O_3 film is employed to passivate the Mo/CISSe rear surface while precipitates formed via chemical bath deposition of CdS are used to generate nanosized point openings. Consequently, Al_2O_3 passivated CISSe solar cells show an increase in the open-circuit voltage (V_{OC}) and short-circuit current density when compared to reference cells with equivalent absorber thicknesses. Notably, a V_{OC} increase of 59 mV contributes to active area efficiencies of 14.2% for rear passivated devices with 0.75 µm thick absorber layers, the highest reported value for submicron-based solution processed, low bandgap CISSe solar cells.

1. Introduction

Photovoltaic (PV) technologies can convert abundant solar energy into electricity economically and with low greenhouse gas lifecycle emissions.[1] For the continued deployment of PV technologies on a global scale, low manufacturing costs and enhanced power conversion efficiencies (PCEs) are urgently needed. For the latter, stacking solar cells with cascading bandgaps (E_g) presents the prospect of overcoming the single-junction Shockley-Queisser efficiency limit of 29.4%.[2] Theoretically, PCEs of ≈46% can be achieved by two-junction tandem devices when the rear, and front sub cell exhibit bandgaps of 0.94 and 1.6 eV, respectively.[3] Here, for the rear cell, the well-established chalcogenide thin-film $CuIn(S,Se)_2$ (CISSe) PV technology offers tunable bandgaps (from 1.0 to 1.53 eV by adjusting the [Se]/[S]+[Se] ratios), low carbon footprint, and device efficiencies up to 19.2% (via sputtering/co-evaporation deposition).[4] Notably, CISSe PV films can be prepared by solution processing methods that disruptively reduce capital equipment expense and energy consumed per square meter of absorber deposited.[5] When integrated with wide bandgap, solution-processable perovskite solar cell technologies, all thin-film perovskite/CISSe tandem devices – attractive as they can be

S. Suresh, A. T. Gidey, T. H. Chowdhury, A. R. Uhl
Laboratory for Solar Energy & Fuels (LSEF)
School of Engineering
University of British Columbia
Kelowna V1V 1V7, Canada
E-mail: alexander.uhl@ubc.ca

S. R. Rondiya
Department of Materials Engineering
Indian Institute of Science
Bangalore 560012, India

L. Tao, J. Liu
Advanced Materials for Energy Storage Lab
School of Engineering
University of British Columbia
Kelowna, BC V1V1V7, Canada

B. Vermang
Institute for Material Research (IMO)
Hasselt University
Diepenbeek B-3590, Belgium

B. Vermang
IMEC Division IMOMEC – Partner in Solliance
Wetenschapspark 1, Diepenbeek B-3590, Belgium

B. Vermang
EnergyVille
Thor Park 8320, Genk B-3600, Belgium

The ORCID identification number(s) for the author(s) of this article can be found under https://doi.org/10.1002/aenm.202303309

DOI: 10.1002/aenm.202303309

manufactured on thin, lightweight, and flexible substrates in a cost-effective manner–promise a path toward high-performance photovoltaics at affordable costs.[5,6]

Compared to a standard ≈2 μm absorber film, the use of submicron CISSe absorber layers further increase the production throughput (lower deposition time), reduces material use (relatively rare indium), and lowers manufacturing costs.[7] Besides, using submicron thick absorber films increases the mechanical flexibility of the resulting solar cell device, allowing for integration in a broad range of consumer-oriented applications including building integrated PV and wearable electronics. However, issues surrounding a highly recombinative rear interface (increased absorber surface-to-volume ratio), and reduced solar spectrum utilization (i.e., thinner absorber films combined with a mediocre-reflective Mo back contact), limit device PCEs to <10%.[6] Moreover, the thickness of submicron absorber films being in the same order of magnitude as the minority carrier diffusion length results in photo-generated carriers to be more exposed to the highly recombinative rear interface.[8–11]

Record PCEs of 26.8% have been reported for c-Si solar cells, attributed to innovations such as surface and contact passivation – that is, by reducing recombination of charge carriers.[12] Similarly, for chalcogenide solar cells, rear surface recombination losses can be mitigated by the application of an Al_2O_3 surface passivation layer at the Mo/CISSe rear interface. For p-type CISSe absorber films, Al_2O_3 has been shown to reduce rear interface recombination by chemical (reducing the interface trap density) and field-effect passivation (high density of negative charges repel and reduce the surface minority charge carrier concentration).[13] Further, Al_2O_3 is an electrical insulator, and consequently, point openings are necessary for electrical connection for the solar cell device. The size and distance (pitch) between the point openings are determined by, among other parameters, the minority carrier diffusion length.[14] When compared to c-Si solar cells, thin film CISSe solar cells exhibit rather short minority carrier diffusion lengths (≈1 μm) and lifetimes (few ns).[7] Thus, scaling from the Si solar cell technology, for carrier diffusion lengths of 0.5–1 μm, point openings with 300–500 nm diameter and pitches between 1.5 and 2.5 μm are necessary for efficient carrier collection.[7]

In the present study, submicron thick CISSe absorber films were fabricated using an *N, N*-dimethylformamide (DMF) and thiourea (TU) – based molecular-ink processing route.[15,16] An ultrathin Al_2O_3 film with nanosized point openings between the rear contact and the CISSe absorber layer was used to reduce the rear interface recombination losses. The Al_2O_3 rear passivated devices with 0.75 μm thick absorber films demonstrated a four-fold increase in the photoluminescence (PL) peak intensity, an average minority lifetime (τ) of 14 ns, and an open-circuit voltage (V_{OC}) of 578.4 mV. Notably, active area efficiencies of 14.2%, and 12.0% were obtained by rear-passivated devices with 0.75 and 0.55 μm thick absorber, respectively, which represents the highest reported values for low bandgap CISSe solar cells with absorbers of equivalent thicknesses and ink-based deposition processes.

2. Results and Discussion

The effects of rear surface passivation on ink-based CISSe solar cells were studied by utilizing a modified rear interface device architecture, that is, a soda lime glass (SLG)/Mo/Al_2O_3 film stack compared with a standard SLG/Mo. Tunneling electron microscopy studies by Vermang et al.,[17] have shown the Al_2O_3 rear passivation layer to withstand the harsh Cu(In,Ga)$(S,Se)_2$ processing conditions (550 °C with Se). Further, nanosized openings are required to facilitate electrical contact while adequately passivating the rear surface.[8] For this, a multistep approach involving 1) deposition of a nanoparticle (NP)-rich CdS layer (by chemical bath deposition (CBD)) on SLG/Mo substrate, 2) atomic layer deposition (ALD) of an Al_2O_3 layer on the CdS NP-rich SLG/Mo substrate, and 3) CdS NP removal from the surface of SLG/Mo/Al_2O_3 film stack by ultrasonic agitation in 10 v/v% HCl was utilized (see **Figure 1**).

Figure 2a depicts the laser scanning confocal microscope image of a NP-rich CdS film deposited on a SLG/Mo substrate. Using this technique, an average CdS NP diameter of 445 ± 50 nm was calculated. Consecutive experiments were conducted to confirm satisfactory NP removal after being coated by an ALD-Al_2O_3 layer. Notably, the highly conformal nature of ALD limited the Al_2O_3 layer thickness to <10 nm, as the NPs embedded in thicker layers could not be removed by our method (see Figure S1a,b, Supporting Information). In addition, >15 nm Al_2O_3 layers were observed to blister (due to outgassing,[7] see Figure S1c, Supporting Information), when subjected to harsh film processing conditions (500–600 °C, under Se vapors). Thus, an ALD-Al_2O_3 thickness of 6 ± 1 nm of was selected for the rear passivated solar cell devices. Figure 2b presents the laser scanning confocal microscopic image of the surface of a – SLG/Mo/ 6 nm Al_2O_3 – film stack, after CdS NP removal. As seen in Figure 2b, the point openings are spaced randomly and are spherical in shape, having an average diameter of 405 ± 20 nm, consistent with previously deposited CdS NPs. The corresponding depth profile of a single nano-sized opening obtained along the indicated line is depicted in Figure 2c. From equivalent analysis of similar samples, the depth of nanosized openings was determined to be 12 ± 4 nm, which indicated etching into an ultrathin CdS layer (see Figure S2, Supporting Information). Furthermore, a similar sample was analyzed by scanning electron microscopy (SEM)-energy-dispersive X-ray (EDX), and the top-view Mo-M, Al-K, and O-K images (see Figure 2d–f) corroborate the formation of the nanosized openings through the Al_2O_3 surface passivation layer.

Following our previous results on comparing the efficiency of DMF-TU-based CISSe devices with different [Cu] contents,[15] a [Cu]/[In] ratio of 1.0 which was shown as the optimum ratio for CISSe devices, was adopted here. Stoichiometric ([Cu]/[In] ≈1.0) DMF-TU-based inks were coated on the standard SLG/Mo, and rear modified SLG/Mo/Al_2O_3 film stacks (see Figure S3, Supporting Information), and thermally treated to build the desired absorber layer thicknesses of 0.55 and 0.75 μm. The molecular ink preparation, precursor film deposition, and precursor film annealing for the absorber layer was carried out in a fume hood, under ambient air conditions. Notably, NaCl (≈0.1 at. %) was added to molecular precursor inks to avoid the "roll-over" effect typical of devices with insufficient sodium in the absorber film,[7] since Al_2O_3 layers act as a barrier for Na diffusion from the SLG substrate. NaF is extensively used in vacuum-processing (via post-deposition treatments), however, it has limited solubility in dimethyl formaldehyde (DMF), which is the solvent used in this work.[18] Consequently, due to NaCl solubility in DMF,[19]

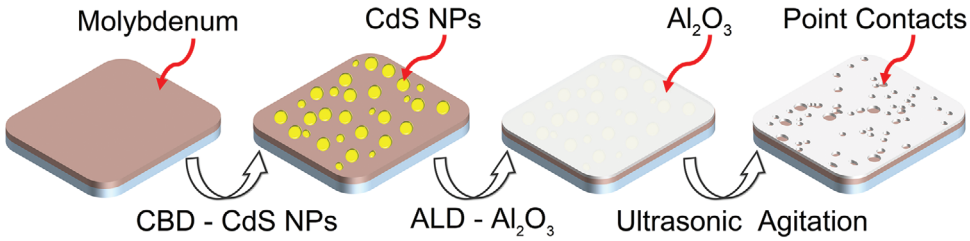

Figure 1. Schematic representation of the process used to create nanosized openings through the surface of the Al_2O_3 passivation layer. In this process, a CdS particle-rich (yellow spheres) layer is grown on the surface of SLG/Mo, which is subsequently coated with an ultrathin layer of Al_2O_3 (white layer). The particles are then removed (ultrasonic agitation) to create nanosized openings in the Al_2O_3 layer.

availability, and wide usage in solution processing routes,[6] NaCl was selected as a sodium source in this work.

In the following, CISSe samples are denoted by the film thickness, in combination with the nanopatterned passivation layer used. For example, Al_2O_3 passivated 0.55 µm absorber films are denoted by 0.55A, and the untreated reference sample by 0.55U. For comparison reasons, both the untreated reference and the Al_2O_3 passivated samples were prepared from the NaCl (0.1 at. %) doped DMF-TU molecular precursor inks. It is expected that excess sodium present on the surface after selenization is washed away by the aqueous solutions during the CdS deposition step.[20] X-ray diffraction peak intensities of the CISSe films on Mo were comparable to those of CISSe films with Al_2O_3 passivation (Figure S4a, Supporting Information), indicating sodium-saturated growth conditions in both cases.[20] Corroborating the latter, an uncoated reference cell without additional NaCl led to equivalent device characteristics (see Figure S4b, Supporting Information).

SEM imaging (see **Figure 3**a–d) determined the average CISSe absorber layer thicknesses for the 0.55U, and 0.75U to be 0.56 ± 0.02 and 0.78 ± 0.02 µm, respectively. Furthermore, large-grained (≈0.55 µm) absorber layers with a smooth film surface (root mean square roughness (σ_{rms}) <30 nm, as determined by profilometry measurements) were observed in both the absorber films. Further, the morphology of the rear passivated CISSe absorber (Figure S5, Supporting Information) was similar to the reference absorber layers of equivalent thickness. Notably, grains for the 0.75U films extended along the thickness of the absorber film. Besides, the grain size was not affected by the thickness of the absorber film, which pointed to sufficient Se supply.[21,22]

To examine whether the Al_2O_3 rear passivation mediated a reduction in the rear surface recombination, time-resolved photoluminescence measurements (TRPL) were conducted on CdS-coated rear surface passivated (0.55A, and 0.75A), and reference samples (0.55U, and 0.75U). In thin CISSe absorber films (<800 nm), charge carriers are generated throughout the whole absorber thickness, and consequently, photoluminescence measurements are sensitive to the recombination at the Mo/CISSe interface.[9,13] **Figure 4**a shows that all the films had a characteristic bi-exponential PL decay (Table S1, Supporting Information), with varying time scales. For the samples with 0.55 µm absorbers, the average minority carrier lifetime increased from 6.3 ± 0.2 ns (extracted following method in,[23]) to 12.2 ± 0.3 ns, from reference to passivated devices. Likewise, increased minority carrier

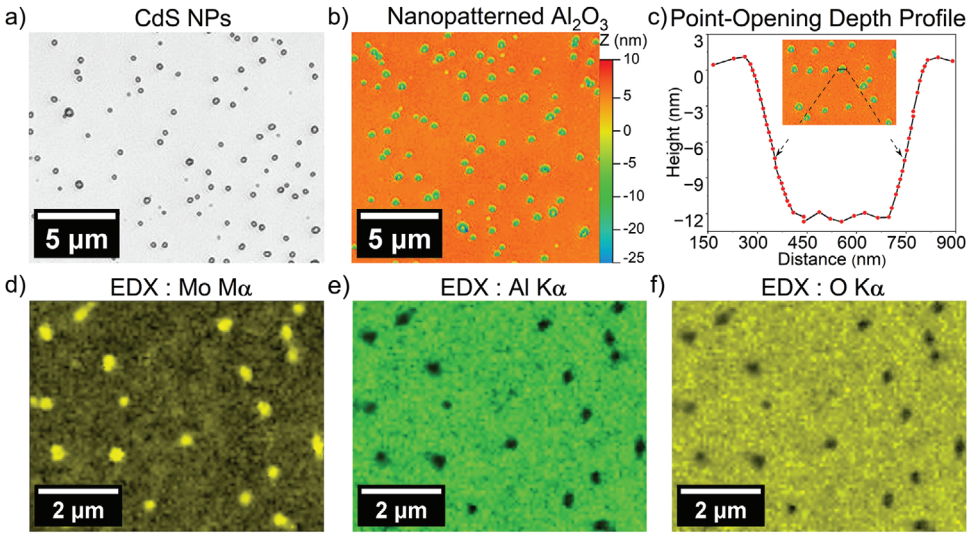

Figure 2. a) A plain light microscopic image of CdS NPs on a SLG/Mo substrate. The particles are randomly dispersed over the surface of the SLG/Mo substrate and have an average diameter of 445 nm. b) Laser scanning confocal microscopic image of the nanosized openings (greenish blue circle) through the Al_2O_3 layer (orange background). c) Depth and lateral profile of a nanosized opening showing the nanosized opening to have an average diameter of 415 nm. d–f) Mo, Al, and O distribution maps from EDX measurements using Mo-M, Al-K, and O-K X-ray lines, respectively.

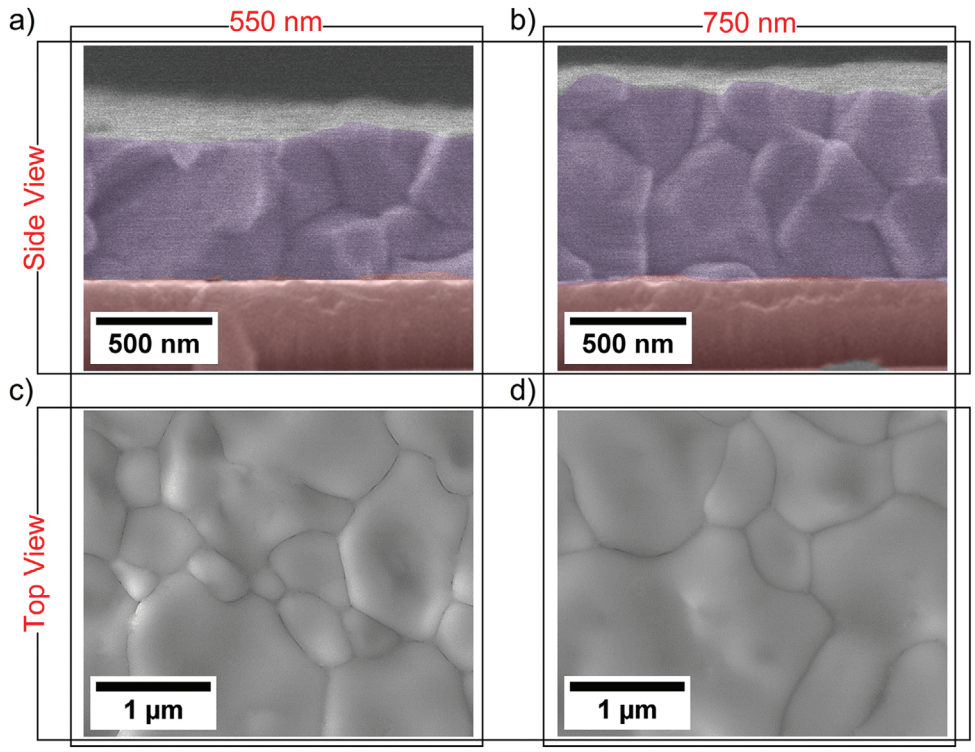

Figure 3. a,b) Side-view, and c,d) Top-view scanning electron microscope images of untreated, 0.55 µm, and 0.75 µm-thick CISSe absorber films, respectively.

lifetimes of 14.3 ± 0.1 ns were obtained by the 0.75A device (versus 9.2 ± 0.1 ns for 0.75U), which indicated that the rear surface passivation schemes indeed improved the carrier lifetimes of the CISSe absorber layer. A fourfold increase in the photoluminescence peak intensity was obtained for the passivated devices (see Figure 4b) when compared with the respective reference devices. First principles calculation by Hsu et al.,[24] showed that Al_2O_3 passivates a Cu(In,Ga)$(S,Se)_2$ surface by 1) reducing ≈35% of the interface defect density, and 2) reducing the rear surface minority carrier concentration due to field effect passivation. Thus, a significant reduction in the surface recombination velocity (and thus rear interface recombination losses) is expected for the Al_2O_3 rear-passivated CISSe surfaces, when compared with the standard Mo/CISSe interface.[7] The enhanced TRPL lifetimes, in combination with increased PL peak intensities would thus point to the effective rear surface passivating capabilities of the Al_2O_3 layer.[8,11] Further, PL data showed emission peaks at ≈0.999 eV for all the absorber film samples.

Motivated by these favorable results, reference solar cell devices were fabricated in the Mo/CISSe/CdS/i-ZnO/ITO/Ni/Al device architecture, with the passivated devices additionally exhibiting a nanopatterned Al_2O_3 layer between the Mo and CISSe layer. Measurements of the charge carrier density and width of the space charge region were obtained from capacitance-voltage (C-V) profiling. Figure 4c shows the apparent charge carrier densities from capacitance-voltage measurements, extracted using conventional methods.[25] A widely reported, U-shaped charge carrier concentration profile was observed for all CISSe solar cell devices.[26] With passivation, the charge carrier densities decreased from 7.8 ± 0.3 × 10^{15} to 7.1 ± 0.5 × 10^{15} cm^{-3} and from 6.2 ± 0.3 × 10^{15} to 5.2 ± 0.2 × 10^{15} cm^{-3} for the 0.55U and 0.75U devices, respectively. Consistent with the decreased free carrier densities for the 0.55A and 0.75A devices, the depletion width of the reference device increased from 293 ± 12 to 296 ± 8 nm and 282 ± 18 to 297 ± 14 nm, for the 0.55U and 0.75U devices, respectively. A wider space charge region improves the long wavelength charge carrier collection; however, lower charge carrier densities result in reduced electric fields across the space charge region.[27] Admittedly the [Na] content may affect the carrier density in the CISSe thin films, however, similar charge carrier densities concentrations for the passivated and reference solar cell devices may suggest identical [Na] in the absorber films.[6] Besides, none of the solar cell devices were fully depleted, as the width of the space charge region was lower than the thickness of the corresponding absorber layers. Figure 4d depicts the temperature dependence of V_{OC} values for reference and rear passivated solar cell devices.

As seen in Figure 4d, the open-circuit voltage and temperature follows a linear relationship in the low-temperature (100–280 K) and near-room-temperature (280–320 K) regimes. A linear fit in the near-room-temperature (280–320K) was employed to extrapolate the recombination activation energy (E_a) of the dominant recombination mechanism (following the method in,[28]). For E_a values lower than the bandgap of the CISSe absorber layer, the dominant recombination is suggested to occur in the interface regions of the device.[29] The losses in the E_a are attributed to band misalignment (e.g., conduction band), fermi level pinning,

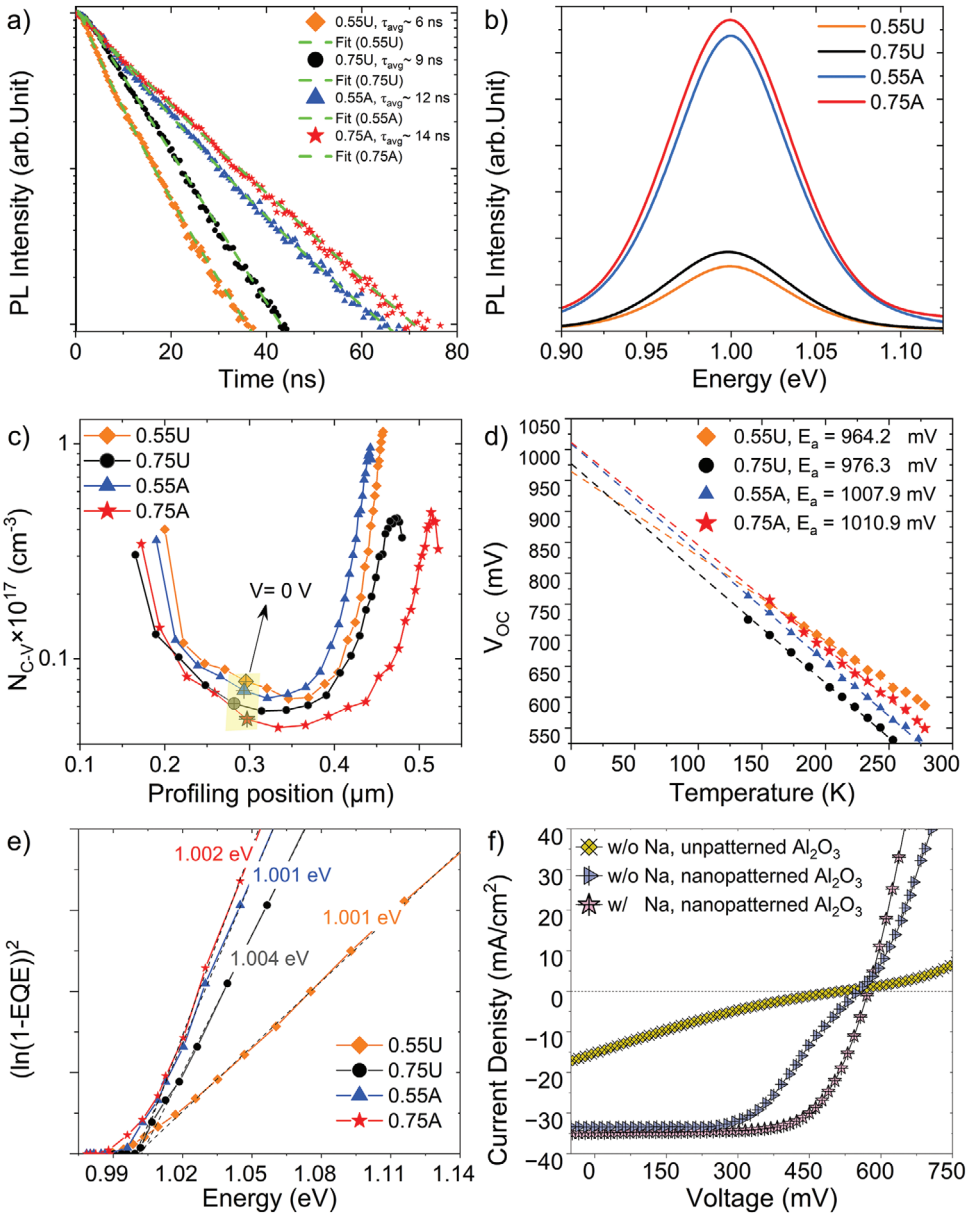

Figure 4. a) Time resolved photoluminescence data, and b) Photoluminescence spectra of CdS-coated, 0.55U, 0.55A, 0.75U, and 0.75A samples, respectively. For the completed solar cell device. c) Comparison of depth profiles of apparent charge carrier density ($N_{C\text{-}V}$) extracted from C-V measurements. d) Extraction of activation energies from temperature dependent V_{OC} measurements for completed solar cell devices. e) Extraction of minimum bandgap from EQE for reference (0.55U, 0.75U), and rear passivated (0.55A, 0.75A devices), and f) *J–V* characteristics of 0.75 µm-thick CISSe solar cell devices, with different device architectures.

or bulk and interface defects. In contrast, for E_a equal E_g, dominant recombination occurs in the bulk absorber film. The differences between PL peaks (indicative of the bandgap energies), and E_a were 36.8, 6.9, 27.7, and 8.9 mV for the 0.55U, 0.55A, 0.75U, 0.75A devices, respectively. A larger difference between E_g and E_a for the reference devices (w.r.t to the passivated device) suggests that dominant recombination occurs at the interface regions of the absorber layer, while the passivated devices were limited by the recombination losses in the bulk absorber. This suggested a reduction in the interface trap states in the passivated absorber films.[28] Further, due to the design of our experiment that focused on the alteration of the rear contact only, we suggest that the reduced interface recombination suggested by our TRPL, PL, and temperature dependent V_{OC} measurements, is indicative of the successful rear surface passivation of our CISSe absorbers with the Al_2O_3 passivation layers. Furthermore, the PL-determined bandgap energies were corroborated by external quantum efficiency (EQE)-determined bandgap energies estimated as 1.001, 1.001, 1.004, and 1.002 eV for the 0.55U, 0.55A, 0.75U, and 0.75A, respectively (see Figure 4e).

Figure 4f shows representative current density–voltage (*J–V*) curves for an un-patterned Al_2O_3 rear surface passivated

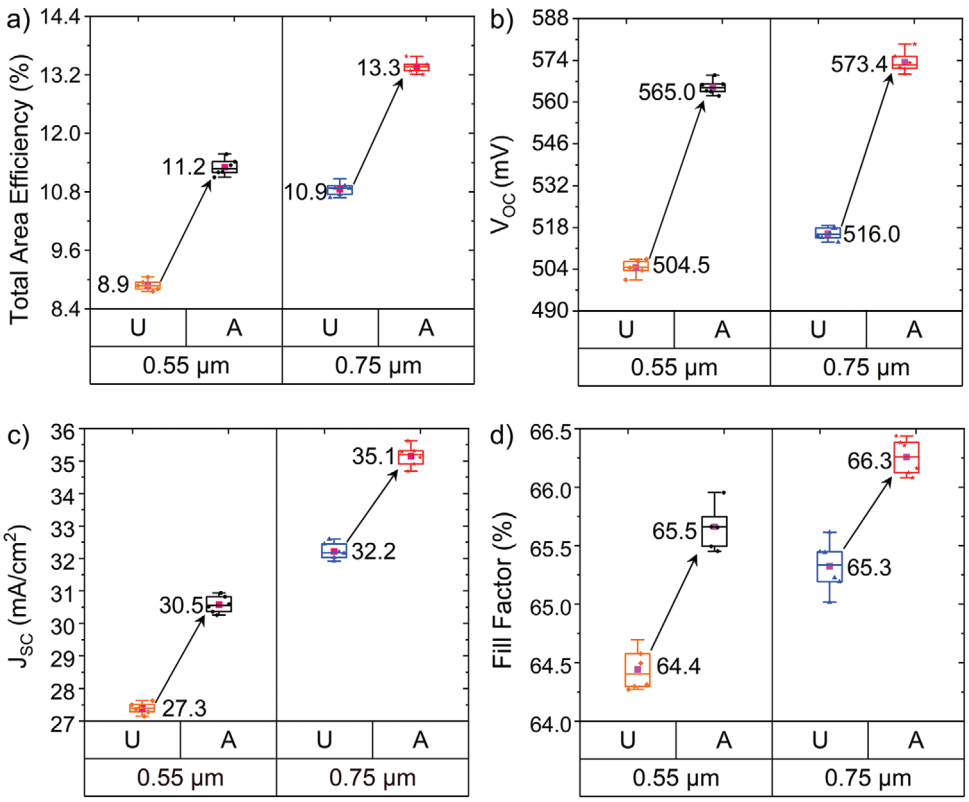

Figure 5. Box plots of the average total area device parameters of the 0.55U, 0.55A, 0.75U, and 0.75A solar cell devices (avg. of 10 cells). The mean values of the respective parameters are provided in the box plots and highlighted as pink boxes.

CISSe solar cell device (absorber thickness 0.75 µm). The low fill factor (FF) (16.1%), and high series resistance (51.3 Ωcm^2) suggests a charge transport barrier at the back contact (Al_2O_3 is a large bandgap (E_g = 7 eV) insulating layer). Figure 4f further shows the *J–V* characteristics of a CISSe device with a 0.75 µm thick, undoped (no NaCl added to the molecular precursor ink) absorber film, and nanopatterned Al_2O_3 layer at the rear interface. The device exhibits low FF (38.1%), and a "roll-over" effect, typical of solar cells with insufficient sodium in the absorber film.[30] This corroborates that Al_2O_3 surface passivated CISSe solar cells require 1) an array of point openings through the Al_2O_3 for appropriate contacting, and 2) an additional supply of sodium. Besides, a reference cell without additional NaCl showed equivalent solar cell characteristics (see Figure S4b, Supporting Information), which was expected as soda lime glass substrates contain plenty of sodium.

Figure 5a–d presents the average device parameters for the reference (0.55U, 0.75U), and nanopatterned Al_2O_3 rear passivated devices (0.55A, 0.75A), including short circuit current density (J_{SC}), V_{OC}, fill factor, and PCE (see Table S2, Supporting Information). Unless otherwise stated, the *J–V* curves and PCE are based on total cell area. For devices with 0.55 µm thick absorbers, the average PCE increased from 8.9 ± 0.1% to 11.3 ± 0.1% with added passivation, with the main enhancements gained in V_{OC} (504.5 ± 2.0 mV versus 565.0 ± 1.4 mV). Further, this 12% (rel.) improvement in the V_{OC} contributed to increased fill factors (64.4 ± 0.2% versus 65.7 ± 0.2%) with comparable series resistances (1.4 Ωcm^2 for 0.55U versus 1.9 Ωcm^2 for 0.55A). Notably, the latter suggests a well-defined and adequate contacting area for the passivated devices and an only minor impact of the lateral distance between point openings on generated charge carriers.

Average PCEs of 10.9 ± 0.1% were obtained by the 0.75U devices, a 22.0% (rel.) increase when compared to 0.55U devices. In addition to insufficient light absorption (optical losses), we expect the absorber layer thickness to increase the impact of the mediocre reflective and passivated Mo/CISSe interface closer to the space charge region of the device.[11] Consequently, the 0.55U devices had an 18.0% (rel.) lower J_{SC}, 2.2% lower V_{OC}, and 1.3% lower FF, compared to 0.75U. For the 0.75A devices (compared to 0.75U), the average V_{OC} and FF increased from 515.9 ± 1.9 to 573.4 ± 3.1 mV and 65.3 ± 0.1% to 66.3 ± 0.1%, respectively. Combined with improvements in J_{SC}, the PCEs increased from 10.9 ± 0.1% to 13.4 ± 0.1%, a 22% (rel.) increase when compared with the 0.75U devices.

Figure 6a shows the active area (see Figure S7, Supporting Information) *J–V* curves of the best-performing CISSe devices in this work with varying absorber film thicknesses. We report a highest PCE of 13.7% (total area), obtained by a 0.75A device having a J_{SC}, V_{OC}, and FF of 34.9 mA cm^{-2}, 578.4 mV, and 67.9%, respectively (active area PCE = 14.2%, J_{SC} = 36.1 mA cm^{-2}). The 0.55A device demonstrated a highest total area PCE of 11.5%, J_{SC} of 30.6 mA cm^{-2}, V_{OC} of 566.1 mV, and FF of 66.5% (active area PCE = 12.0%, J_{SC} = 31.8 mA cm^{-2}). Calculated active area J_{SC} values from EQE were 30.4, 32.1, 34.1 and 36.4 mA cm^{-2}, for the 0.55U, 0.55A, 0.75U, and 0.75A device, respectively, consistent with the *J–V* results (see Figure 6b).

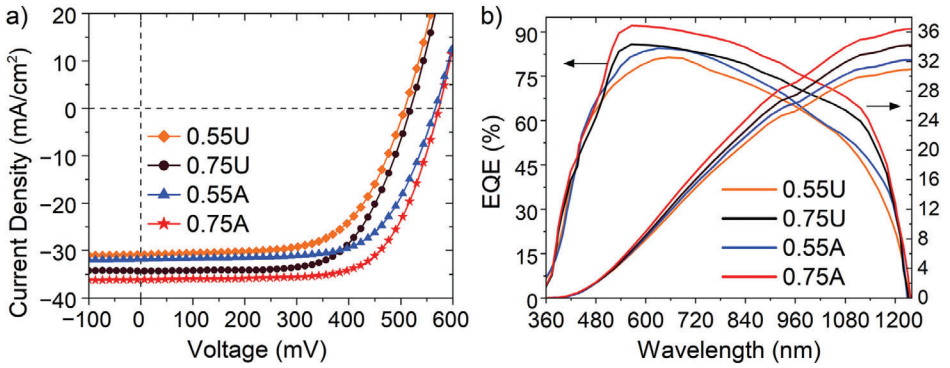

Figure 6. a) Active area *J–V* characteristics of the best performing reference (0.55U, 0.75U) and rear-passivated (0.55A, 0.75A) devices. b) EQE data of the respective champion devices.

Capacitance-voltage measurements (see Figure 4c) suggested the passivated devices to have similar, or marginally lower charge carrier concentration when compared with the respective reference devices. Hence, the V_{OC} improvements may not be ascribed to the changes in the charge carrier density values. To better understand the improved V_{OC} for the passivated solar cell devices, the reverse saturated current (J_0) was calculated (using methods described in,[31]) to be 3.4×10^{-6}, and 1.1×10^{-6} A cm^{-2} values for the 0.55U and 0.75U devices, respectively and 1.3×10^{-7} and 4.8×10^{-7} A cm^{-2} for the 0.55A, and 0.75A devices, respectively. This significant reduction in the reverse saturation current by 1 order of magnitude indicates a reduction in the recombination losses with passivation, which is consistent with observed increases in the minority lifetime and a fourfold increase in the PL response for the passivated device (see Figure 4a,b above). The EQE data for the highest efficiency devices with varying absorber film thicknesses is shown in Figure 6b. Compared to 0.75U, the EQE response decrease in the near-infrared region for the 0.55U may stem from incomplete absorption of incident light due to thinner absorber films. Notably, the spectral response improved in the 500 to 1200 nm wavelength range for the passivated devices when compared with the respective reference devices. The improvements to the J_{SC} may thus be ascribed to increased average minority carrier diffusion length (due to field effect passivation) and a reduction in the rear interface defect density (chemical passivation), rather than to marginal optical benefits through improved reflection (ultrathin Al_2O_3). This theory is further corroborated by the increased minority carrier lifetimes and space charge region width from TRPL and C-V measurements, respectively, that indicated improved carrier collection. Notably, our champion cell V_{OC} of 578.4 mV exceeds values of the currently reported highest efficiency DMF-TU-based device, see **Table 1**), pointing to the excellent charge carrier management in our rear surface passivated devices.[5,6] To the best of the authors knowledge, our champion device active area efficiencies of 12.0%, and 14.2% are the highest reported efficiencies for submicron (0.56 and 0.78 µm, respectively) non-vacuum-based CISSe devices (Table 1).[5] Further improvements are expected by applying well-order rear contacting structures (e.g., using lithography to generate well-controlled grids of nanosized point contact openings), bandgap gradients, and application of anti-reflective coatings (typical +5% improvement with MgF_2 to yield 14.9% PCE).

3. Conclusion

In conclusion, a facile rear surface passivation scheme was developed and implemented for solution-processed CISSe solar cell devices for the first time. A 6 nm layer of ALD-Al_2O_3 was used to passivate the Mo/CISSe rear interface, while nanosized spherical precipitates formed during CBD of CdS were used to generate point contact openings. We believe that the presented rear surface passivation method is particularly beneficial for ink-based chalcogenide deposition processes, which are inherently prone to the formation of thin absorbers and extensive $MoSe_2$. By carefully tailoring the Al_2O_3 film thickness, and optimizing the contacting area at the rear interface, record active area efficiencies of 14.2% (without MgF_2) were obtained for solution

Table 1. Active area solar cell performance for devices with solution processed $CuIn(S,Se)_2$ absorbers with various absorber film thicknesses.

Device	$t_{absorber}$ [µm]	PCE [%]	V_{OC} [mV]	FF [%]	J_{SC} [mAcm^{-2}]	J_{SC} (EQE) [mAcm^{-2}]
This Work	0.56	12.0	566	66.8	31.8	32.3
This Work	0.78	14.2	578	67.9	36.1	36.4
Xin et al.,[32]	1.2	14.5*	520	72.5	38.5	37.1
Ahn et al.,[33]	3.0	14.4*	564	68.8	37.1	N/A
Uhl et al.,[16]	1.2	13.8*	518	70.3	37.9	36.4
Clark et al.,[19]	2.2	13.4*	512	71.0	36.9	37.0

*Device with anti-reflective coating

processed CISSe devices with 0.75 µm absorber films, exhibiting V_{OC} of up to 578.4 mV for a 1.0 eV bandgap absorber (>25% PCE improvement to baseline device). Furthermore, ink-deposition-based routes for chalcogenide film fabrication are typically associated with high absorber roughness and the formation of additional porous, fine-grained layers due to residual impurities.[21,34] A limiting factor in development of perovskite/CISSe tandem solar cells has been the relatively rough (σ_{rms} > 100 nm) CISSe top surface, with lateral feature sizes in the order of ≈500 nm. In this work, void-free, large grained (≈500 nm), smooth absorber film surfaces (σ_{rms} < 30 nm) were obtained, challenging the traditional conceptions of inherently inferior material properties for molecular-ink-based absorber films, and thus, paving the way for highly efficient and cost-competitive, printed thin-film tandem solar cells (i.e., CISSe/perovskite).

Supporting Information

Supporting Information is available from the Wiley Online Library or from the author.

Acknowledgements

The authors would like to acknowledge that this work was conducted on the traditional, ancestral, and unceded territory of the Syilx Okanagan Nation (Kelowna). S.S, T.H.C, A.G.T, and A.R.U acknowledge the financial support provided by the Natural Sciences and Engineering Research Council of Canada (NSERC), through grants RGPIN-2019-05489 and DGECR-2019-00450 as well as the Canada Foundation for Innovation (CFI) and the British Columbia Knowledge Development Fund (BCKDF) through grants 39081 and 42549. A.R.U. further acknowledges funding through the UBC Okanagan Principal's Research Chair program. S.R.R acknowledges the support of the Department of Materials Engineering, Indian Institute of Science (IISc), Bangalore, India, and the Science and Engineering Research Board (SERB), Govt. of India under grant agreement No. EEQ/2022/000697. B.V. acknowledges funding from the European Union's Horizon 2020 research and innovation program under grant agreement No. 850937. Dr. Liu's work was supported by the Natural Sciences and Engineering Research Council of Canada (NSERC), Canada Foundation for Innovation (CFI), BC Knowledge Development Fund (BCKDF), Killam Research Accelerator Fellowship Program, and the University of British Columbia (UBC).

Conflict of Interest

The authors declare no conflict of interest.

Data Availability Statement

The data that support the findings of this study are available from the corresponding author upon reasonable request.

Keywords

CIS, doping, non-vacuum, passivation, photovoltaics, solar cells, thin films

Received: October 1, 2023
Revised: November 29, 2023
Published online:

[1] J. S. Kikstra, Z. R. J. Nicholls, C. J. Smith, J. Lewis, R. D. Lamboll, E. Byers, M. Sandstad, M. Meinshausen, M. J. Gidden, J. Rogelj, E. Kriegler, G. P. Peters, J. S. Fuglestvedt, R. B. Skeie, B. H. Samset, L. Wienpahl, D. P. Van Vuuren, K.-I. Van Der Wijst, A. Al Khourdajie, P. M. Forster, A. Reisinger, R. Schaeffer, K. Riahi, *Geosci. Model Dev.* **2022**, *15*, 9075.
[2] A. Richter, M. Hermle, S. W. Glunz, *IEEE J. Photovoltaics* **2013**, *3*, 1184.
[3] A. D. Vos, *J. Phys. D: Appl. Phys.* **1980**, *13*, 839.
[4] T. Feurer, R. Carron, G. Torres Sevilla, F. Fu, S. Pisoni, Y. E. Romanyuk, S. Buecheler, A. N. Tiwari, *Adv. Energy Mater.* **2019**, *9*, 1901428.
[5] S. Suresh, A. R. Uhl, *Adv. Energy Mater.* **2021**, *11*, 2003743.
[6] S. Suresh, D. J. Rokke, A. A. Drew, E. Alruqobah, R. Agrawal, A. R. Uhl, *Adv. Energy Mater.* **2022**, *12*, 2103961.
[7] B. Vermang, V. Fjällström, J. Pettersson, P. Salomé, M. Edoff, *Sol. Energy Mater. Sol. Cells* **2013**, *117*, 505.
[8] B. Vermang, J. T. Watjen, C. Frisk, V. Fjallstrom, F. Rostvall, M. Edoff, P. Salome, J. Borme, N. Nicoara, S. Sadewasser, *IEEE J. Photovoltaics* **2014**, *4*, 1644.
[9] S. Bose, J. M. V. Cunha, S. Suresh, J. De Wild, T. S. Lopes, J. R. S. Barbosa, R. Silva, J. Borme, P. A. Fernandes, B. Vermang, P. M. P. Salomé, *Sol. RRL* **2018**, *2*, 1800212.
[10] T. S. Lopes, J. P. Teixeira, M. A. Curado, B. R. Ferreira, A. J. N. Oliveira, J. M. V. Cunha, M. Monteiro, A. Violas, J. R. S. Barbosa, P. C. Sousa, I. Çaha, J. Borme, K. Oliveira, J. Ring, W. C. Chen, Y. Zhou, K. Takei, E. Niemi, F. L. Deepak, M. Edoff, G. Brammertz, P. A. Fernandes, B. Vermang, P. M. P. Salomé, *npj Flexible Electron.* **2023**, *7*, 4.
[11] S. Suresh, J. de Wild, T. Kohl, D. G. Buldu, G. Brammertz, M. Meuris, J. Poortmans, O. Isabella, M. Zeman, B. Vermang, *Thin Solid Films* **2019**, *669*, 399.
[12] M. A. Green, E. D. Dunlop, M. Yoshita, N. Kopidakis, K. Bothe, G. Siefer, X. Hao, *Prog. Photovoltaics* **2023**, *31*, 651.
[13] R. Kotipalli, B. Vermang, J. Joel, R. Rajkumar, M. Edoff, D. Flandre, *AIP Adv.* **2015**, *5*, 107101.
[14] I. L. Repins, W. K. Metzger, C. L. Perkins, J. V. Li, M. A. Contreras, *IEEE Trans. Electron Devices* **2010**, *57*, 2957.
[15] S. Suresh, D. Abou-Ras, T. H. Chowdhury, A. R. Uhl, *Sol. RRL* **2023**, *7*, 2300437.
[16] A. R. Uhl, A. Rajagopal, J. A. Clark, A. Murray, T. Feurer, S. Buecheler, A. K.-Y. Jen, H. W. Hillhouse, *Adv. Energy Mater.* **2018**, *8*, 1801254.
[17] B. Vermang, V. Fjallstrom, X. Gao, M. Edoff, *IEEE J. Photovoltaics* **2014**, *4*, 486.
[18] H. Xiang, P. Liu, W. Wang, R. Ran, W. Zhou, Z. Shao, *J. Mater. Sci. Technol.* **2022**, *113*, 138.
[19] J. A. Clark, A. Murray, J.-M. Lee, T. S. Autrey, A. D. Collord, H. W. Hillhouse, *J. Am. Chem. Soc.* **2019**, *141*, 298.
[20] H. Xin, S. M. Vorpahl, A. D. Collord, I. L. Braly, A. R. Uhl, B. W. Krueger, D. S. Ginger, H. W. Hillhouse, *Phys. Chem. Chem. Phys.* **2015**, *17*, 23859.
[21] A. R. Uhl, P. Fuchs, A. Rieger, F. Pianezzi, C. M. Sutter-Fella, L. Kranz, D. Keller, H. Hagendorfer, Y. E. Romanyuk, F. Lamattina, S. Yoon, L. Karvonen, T. Magorian-Friedlmeier, E. Ahlswede, D. Vangenechten, F. Stassin, A. N. Tiwari, *Prog. Photovoltaics* **2015**, *23*, 1110.
[22] A. R. Uhl, J. K. Katahara, H. W. Hillhouse, *Energy Environ. Sci.* **2016**, *9*, 130.
[23] B. Ohnesorge, R. Weigand, G. Bacher, A. Forchel, W. Riedl, F. H. Karg, *Appl. Phys. Lett.* **1998**, *73*, 1224.
[24] W.-W. Hsu, J. Y. Chen, T.-H. Cheng, S. C. Lu, W.-S. Ho, Y.-Y. Chen, Y.-J. Chien, C. W. Liu, *Appl. Phys. Lett.* **2012**, *100*, 023508.
[25] J. T. Heath, J. D. Cohen, W. N. Shafarman, *J. Appl. Phys.* **2004**, *95*, 1000.
[26] P. M. P. Salomé, A. Hultqvist, V. Fjällström, M. Edoff, B. Aitken, K. Vaidyanathan, K. Zhang, K. Fuller, C. Kosik Williams, *IEEE J. Photovoltaics* **2013**, *3*, 852.
[27] U. Rau, H. W. Schock, *Appl. Phys. A* **1999**, *69*, 131.

[28] T. Eisenbarth, T. Unold, R. Caballero, C. A. Kaufmann, H.-W. Schock, *J. Appl. Phys.* **2010**, 107.
[29] P. Blood, J. W. Orton, *The Electrical Characterization of Semiconductors : Majority Carriers and Electron States*, Academic Press, London, **1992**.
[30] B. Vermang, J. T. Wätjen, V. Fjällström, F. Rostvall, M. Edoff, R. Kotipalli, F. Henry, D. Flandre, *Prog. Photovoltaics* **2014**, *22*, 1023.
[31] S. S. Hegedus, W. N. Shafarman, *Prog. Photovoltaics* **2004**, *12*, 155.
[32] J. Jiang, R. Giridharagopal, E. Jedlicka, K. Sun, S. Yu, S. Wu, Y. Gong, W. Yan, D. S. Ginger, M. A. Green, X. Hao, W. Huang, H. Xin, *Nano Energy* **2020**, *69*, 104438.
[33] Y. Siddique, K. Son, T. R. Rana, S. D. H. Naqvi, P. M. Hoang, A. Ullah, H. Tran, S. M. Lee, S. Hong, S. K. Ahn, I. Jeong, S. Ahn, *Energy Environ. Sci.* **2022**, *15*, 1479.
[34] A. R. Uhl, C. Fella, A. Chirila, M. R. Kaelin, L. Karvonen, A. Weidenkaff, C. N. Borca, D. Grolimund, Y. E. Romanyuk, A. N. Tiwari, *Prog. Photovoltaics* **2012**, *20*, 526.